ChemElectroChem

Research Article
doi.org/10.1002/celc.202400231

Chemistry Europe
European Chemical Societies Publishing

www.chemelectrochem.org

Electroreduction of CO_2 by Hybrid Cu-TiO_2/rGO Catalyst: Qualitative Detection of Products using Rotating Ring Disc Electrode

Adefunke O. Koyejo,[a, b] Xia Chu,[b] Lokesh Kesavan,[b] Pia Damlin,[b] and Carita Kvarnström*[b]

The electrochemical reduction of CO_2 ($ERCO_2$) to valuable chemicals such as acetic acid/acetate offers a promising route to revolutionize chemical production and enhance sustainability. Here, we report the hydrothermal preparation of an electrocatalyst consisting of copper/titanium dioxide/reduced graphene oxide (Cu-TiO_2/rGO) for $ERCO_2$ in aqueous medium. The metal-support (TiO_2/rGO) was pre-synthesized by combining an aqueous solution of TiO_2 and GO in an autoclave at 150 °C for 20 h. Then TiO_2/rGO was added to synthesized Cu colloid formed through the reduction of copper (II) nitrate trihydrate resulting in the formation of Cu-TiO_2/rGO. The Cu-TiO_2/rGO hybrid nanocomposite was fully characterized using spectroscopic and microscopic techniques. This study explored the versatility of the rotating ring-disc electrode (RRDE) as an *in situ* electroanalytical tool for the selective detection of products formed during $ERCO_2$. The well-designed hybrid electrocatalyst, containing Cu^0/Cu^+ active sites, facilitated the eight-electron transfer for acetic acid (AA) formation at low potentials. AA formation was detected on the RRDE and validated by conventional NMR and HPLC techniques. This work highlights and expands the scope of selective hydrogenation of CO_2 towards value-added products.

Introduction

The use of CO_2 as feedstock for the production of value-added fuels and chemicals is a promising pathway for development of renewable energy storage and reduction of carbon emissions. The electrochemical reduction of CO_2 ($ERCO_2$), using heterogeneous catalysts, has the potential of providing diverse products such as carbon monoxide, formic acid, methanol, and other value-added chemicals.[1] However, the product formed depends on the choice of catalyst, electrolyte, electrode material and pH. The idea of reducing CO_2 is propelled by an ambition to move from a fossil fuel-based to a renewable energy-based economy.

Various metal-based nanoparticles, including Sn, Pb, In, and Cu, have been studied for CO_2 reduction. Nobel metals like Ag, Au and Pd have been reported to be highly selective towards C_1 products (CO and CH_2O_2).[2] However, the non-noble, low-cost Cu has gained attention due to its ability to generate C_2 products from $ERCO_2$. Nevertheless, its poor selectivity and stability has been a major limitation. On the other hand, $ERCO_2$ in aqueous media is associated with poor selectivity due to the competing HER. Thus, to retard HER and improve the selectivity of Cu catalysts, efforts have been focused on catalyst modification. Strategies to modify and improve the catalytic activity of Cu towards $ERCO_2$ include alloying (Ag–Cu, Pd–Cu, Au–Cu, Co–Cu),[3] and incorporating metal oxide (such as TiO_2)[4] or carbon substrates (e.g., graphene, carbon black and carbon nanotube)[5] as support material to disperse, stabilize and avert the deactivation of metal nanoparticles. TiO_2 is a semiconductor material that has been used extensively in electrocatalysis and photocatalysis due to its stability, photo-corrosion resistance, and oxidizing activity.[6] Literature reports that TiO_2 also promotes CO_2 reduction by enhancing CO_2 adsorption and stabilizing the intermediate formed during $ERCO_2$.[7] On the other hand, graphene, and its derivatives (graphene oxide (GO) and reduced graphene oxide (rGO)) are also ideal support materials due to their high surface area, excellent electronic conduction, and ease of functionalization.[8] rGO particularly provides carbon vacancies that enhances even further the adsorption, intercalation and activation of ions and molecules.[9] Some of the results reported for $ERCO_2$ using hybrid composites consisting of Cu, TiO_2 or rGO (carbon substrates) have resulted in the formation of methanol, acetate/acetic acid, and formate during photochemical and electrochemical CO_2 reduction.[10–14] The selective formation of acetic acid during $ERCO_2$ have been reported using Cu-based catalysts. For example, Genovese *et al.* reported the selective formation of acetic acid on Cu-CNT electrocatalyst with traces of formic acid and methanol.[15] Zhu *et al.* also reported lower overpotential and increased formation of acetic acid on Cu-Cu_2O/Cu electrode.[16] Zhu *et al.* attributed this to the synergy between Cu^1/Cu^0 active sites. The current approach to the synthesis of acetic acid is through the carbonylation of methanol. Hence, the reduction of CO_2 to

[a] *A. O. Koyejo*
University of Turku graduate school (UTUGS), Doctoral Programme in EXACT Sciences (EXACTUS), Turku, Finland

[b] *A. O. Koyejo, X. Chu, Dr. L. Kesavan, Dr. P. Damlin, Prof. C. Kvarnström*
University of Turku, Department of Chemistry, Materials Chemistry, Henrikinkatu 2, FI-20014 Turku, Finland
E-mail: carita.kvarnstrom@utu.fi

Supporting information for this article is available on the WWW under https://doi.org/10.1002/celc.202400231

acetic acid is a desirable route required to transition from fossil fuels to renewable energy sources.[17]

Although, $ERCO_2$ product distribution depends on the nature of the catalyst and the experimental conditions, analytical techniques play a crucial role in the identification of the product species. Several literature reports have used offline techniques such as gas chromatography (GC), high performance liquid chromatography (HPLC) and nuclear magnetic resonance (NMR) spectroscopy. The time-consuming nature of these analytical techniques possess a limitation on their utilization. Consequently, there is a need for an online and quick product detection method. Several online techniques, including *in situ* spectroscopic techniques,[18–20] differential electrochemical mass spectroscopy (DEMS) and rotating ring disk electrode (RRDE) voltammetry, have been reported for $ERCO_2$.[21]

The RRDE is a valuable, quick *in situ* electroanalytical detection tool that provides insight on the products generated at the disc, while ensuring controlled mass transport conditions.[22] The RRDE consists of a disc and a ring that serve as a primary and a secondary working electrode respectively. This electroanalytical tool is particularly useful when the amount of product generated within the electrolyte bulk solution is too low. The RRDE then takes advantage of the high product concentration near the electrode surface to detect products *in situ* at the ring. The RRDE has been widely used in oxygen reduction reactions (ORR).[23–25] Although there is increasing development in the use of RRDE for $ERCO_2$, literature reports have majorly explored the use of plain or unmodified metal electrode.[26,27] Thus, there is limited studies[28,29] on $ERCO_2$ by a catalyst modified electrode using RRDE. Therefore, motivated by the properties and literature reports of GO, TiO_2, and Cu for $ERCO_2$, as well as the uniqueness of the RRDE technique, we investigated the hybrid electrocatalyst Cu-TiO_2/rGO for $ERCO_2$.

In this study, the hybrid nanocomposite of Cu-TiO_2/rGO was hydrothermally synthesized. Firstly, commercial TiO_2 was hydrothermally incorporated with GO, this involved the simultaneous reduction of GO to rGO to form TiO_2/rGO. Further, copper nanoparticles (Cu NPs) were embedded on the TiO_2/rGO through $NaBH_4$ reduction method, to form Cu-TiO_2/rGO. The electrocatalytic performance of the synthesized nanocomposites were evaluated for $ERCO_2$. Subsequently, we employed the RRDE as an electrochemical tool to study the formation of products during $ERCO_2$ on the Cu-TiO_2/rGO catalyst. Reduction was achieved on the GC disc (primary working electrode), while product generation was detected on the Pt ring (secondary working electrode). This study reports the selectivity and detection of acetic acid (CH_3COOH (AA)) as the primary product generated from $ERCO_2$ on the Cu-TiO_2/rGO. We show the RRDE as a quick and sensitive detection tool for the screening of catalyst for electrochemical applications.

Experimental

Reagents

Potassium bicarbonate ($KHCO_3$, ≥99.7%, JT Baker), potassium chloride (KCl, Acros Organics), copper (II) nitrate trihydrate ($Cu(NO_3)_2 \cdot 3H_2O$, 99%, Merck), titanium dioxide (TiO_2, 98% Degussa, P25), sodium borohydride ($NaBH_4$, Merck), polyvinyl alcohol (PVA, Merck), Nafion (5% solution, Aldrich), formic acid (CH_2O_2, ≥95% Sigma-Aldrich), acetic acid ($C_2H_4O_2$, ≥99.7% ACS reagent), isopropyl alcohol (IPA, 99.5% Sigma-Aldrich), graphene flakes (99.9% purity, Alfa Aesar) were used as reagents. All reagents were commercially available and used without further purification, and all solutions were prepared using deionized Milli-Q water.

Materials Preparation

Synthesis of TiO_2/rGO

Graphene oxide (GO) was prepared from natural graphite flakes by the modified Hummers method[30] according to a procedure extensively elaborated and reported earlier by us.[31] The total GO concentration was 5 mg/ml. TiO_2/rGO was synthesized by a hydrothermal method, similar to the one reported in literature.[32] In brief, 1 ml of 5 mg/ml GO solution was first treated with ultrasonication at 9 kHz (VWR ultrasonic cleaner) for 1 h to separate the graphene oxide sheets. Then 95 mg of TiO_2 (95 wt%) was dispersed in 40 ml deionized water and sonicated for 15 min. After that, the TiO_2 solution was added slowly to the GO dispersion and stirred for another 1 h. TiO_2/rGO (95:5 wt%) mixture was then treated hydrothermally in a Teflon lined autoclave at 150 °C for 20 h (this method simultaneously reduced GO). The resulting solution was washed with deionized water and dried at 25 °C for 20 h. The resulting powder was collected and labelled TiO_2/rGO.

Synthesis of Cu-TiO_2/rGO

Cu-TiO_2/rGO was synthesized by an $NaBH_4$ reduction method, which has been earlier reported by us.[33] First, 6 mg of PVA was dissolved in 10 ml deionized water at 60 °C. Then the desired amount of an aqueous solution of $Cu(NO_3)_2 \cdot H_2O$ and PVA were mixed in a 3 necked round bottom flask equipped with a nitrogen inlet with constant stirring. Then freshly prepared $NaBH_4$ (0.1 M) was added to the mixture and stirred for 30 min. A colour change from colourless to brown was observed. Subsequently, previously synthesized TiO_2/rGO (95:5 wt%) powder was added to the Cu colloid and stirred for 1 h. The mixture was filtered and washed with deionized water. The resulting Cu-TiO_2/rGO powder was dried at 110 °C in a vacuum oven for 20 h. The concentration of Cu in the final hybrid composite was 2 wt%.

Electrode Preparation

Before each experiment, the GC disc and Pt ring electrodes were polished mechanically using Struers (DP-paste P) diamond paste of 15, 6, 3, 1 and $^1/_4$ μm particle sizes. Then rinsed with quartz distilled water and ethanol. The Pt electrode was further cleaned electrochemically by potential cycling from 0 to 1.5 V vs. Ag/AgCl at 50 mVs^{-1} for 50 cycles in 0.5 m H_2SO_4 until a steady state CV was observed.

1 mg/ml of catalyst was dissolved in ethanol and treated with ultrasonication for 15 min to form a homogeneous dispersion. Then 20 μL (for LSV measurements) or 40 μL (40 μg→0.8 μg Cu) (for RRDE measurements) of the dispersion was drop casted on the freshly

cleaned glassy carbon electrode (GCE) and dried at room temperature. Finally, 5 μL of Nafion solution was coated on the deposited catalyst layer and dried at room temperature.

Electrochemical Measurement Using Rotating Ring-Disk Electrode (RRDE)

The electrochemical measurements were performed in a conventional three-electrode system powered by an Iviumstat bipotentiostat equipped with a rotator. The working electrode (WE) was a catalyst modified rotating ring-disc electrode. The RRDE glassy carbon disc (primary WE) with a diameter of 4 mm (A = 0.2475 cm^2) and a Pt ring (secondary WE) with an internal diameter of 5 mm and an external diameter of 7 mm (A = 0.1866 cm^2). A Pt mesh of 1.5 cm by 1.5 cm was used as a counter electrode; a silver wire coated with Ag/AgCl served as a pseudo reference electrode and 0.5 M $KHCO_3$ solution was used as an aqueous electrolyte. The reference electrode was calibrated for every electrochemical measurement using $K_3[Fe(CN)_6]$ redox couple ($E_{1/2}$ (Fe/Fe^+) = 0.248 V).

Prior to each experiment, the electrolyte solution was purged with N_2 (this was used for the blank experiments) for 20 min and then saturated CO_2 gas for 30 min (at a flow rate of 40 SCCM). After the saturation of CO_2, the pH of the electrolyte medium dropped from pH 8.2 to pH 7.2 as measured with a HANNA edge HI-2020-02 pH meter. The RRDE was assembled and inserted into the electrochemical glass cell and a rotation of 1600 rpm was applied to dispel gas bubbles away from the disc surface. In the electrochemical experiments a combination of linear sweep voltammetry (LSV), cyclic voltammetry (CV) and chronoamperometric (CA) techniques were applied in N_2 or CO_2 saturated 0.5 M $KHCO_3$ electrolyte solution at various potentials *vs.* Ag/AgCl. All potentials measured against Ag/AgCl electrode were converted to reversible hydrogen electrode (RHE) values to correct the pH differences between N_2 and CO_2 saturated solutions using (Eq. (1)).

$$E_{RHE} = E_{Ag/AgCl} + 0.059pH + E^{o}_{Ag/AgCl(sat)} \quad (1)$$

Where $E_{Ag/AgCl}$ denotes the experimental data measured against the Ag/AgCl electrode and $E^{o}_{Ag/AgCl}$is 0.1976 at 25 °C.

Thus, two set of experiments were conducted to enhance the $ERCO_2$ using RRDE:

i). The first set of experiment involved the calibration of product species using the rotating ring electrode (RRE) method on the Pt ring. Since AA was our product of interest and its detection has been confirmed in earlier literature alongside formic acid over Cu/Cu_2O based electrocatalyst, the identification of AA and FA was investigated on the Pt ring. To maintain consistent pH conditions, the electrochemical response of 0.1 M AA/CO_2 and 0.1 M FA/CO_2 mixtures in 0.5 M $KHCO_3$ was recorded on the Pt ring from 0 to 1.7 V *vs.* RHE at a scan rate of 100 mVs^{-1} and a rotation speed of 1600 rpm. The GC disc was off.

ii). The second set of experiment involved an *in situ* detection of products formed for $ERCO_2$ in 0.5 M $KHCO_3$ on Cu-TiO_2/rGO catalyst. The Pt ring served as a secondary working electrode to detect the products generated during $ERCO_2$ at the ring. The *in situ* detection was achieved by scanning the ring (from 0.6 to 1.7 V *vs.* RHE) at a scan rate of 100 mVs^{-1} and a rotation speed of 1600 rpm while keeping the disc at suitable constant potentials where $ERCO_2$ is expected to generate products.

Chronoamperometry test was performed for 60 min in a CO_2 saturated 0.5 M $KHCO_3$ electrolyte solution. The catalyst modified GC disc electrode served as working electrode. The ring was disconnected to prevent product oxidation after which 2 mL of samples were collected for HPLC and NMR analysis.

Collection Efficiency (N) of RRDE

The collection efficiency (*N*) of the RRDE was determined experimentally from the ratio of ring ($i_{L,RING}$) to disc current ($i_{L,DISC}$) in the plateau region during the oxidation and reduction of 10 mM $K_3[Fe(CN)_6]$ in 0.5 M $KHCO_3$ purged with N_2 at a rotation speed of 1600 rpm. *N* was calculated (Eq. (2)) to be 0.3 and remained consistent throughout every experiment reported in this work. The RRDE electrode was calculated to have a 30% collection efficiency.

$$N_{empirical} = \left| \left(\frac{i_{L.RING}}{i_{L.DISC}} \right) \left(\frac{n_D}{n_R} \right) \right| \quad (2)$$

Where n_D and n_R indicate the number of electrons exchanged at the disk and ring ($n_D = n_R$).

Material Characterization

The crystalline phases of the composite materials were analyzed using a Malvern PANalytical powder X-ray diffractometer (XRD), with a Cu Kα radiation of 1.5418 Å. Measurement took place at 10–80° 2θ Bragg-angles at room temperature.

The Fourier-transform infrared (FTIR) spectra of powder samples were recorded at room temperature within the spectral region of 4000 to 450 cm^{-1} using a Bruker Vertex 70 FTIR spectrometer equipped with a Harrick VideoMVPTM diamond ATR accessory and deuterated-triglycine sulfate (DTGS) detector. The FTIR spectra were recorded after a total of 32 scans with a resolution of 4 cm^{-1}.

The microscopic morphology of the catalysts was analysed using transmission electron microscopy (TEM: JEM-1400 plus). The solid catalyst samples were dispersed in ethanol and dropped on a carbon polymer coated Cu grid. The grids were then dried using hot air gun before inserting into a high vacuum chamber.

The electronic state of Cu (Cu 2p) was recorded using a Thermo Scientific Nexsa Surface Analysis System equipped with an Al Kα X-ray source. Survey scans and high-resolution region scans were measured. The XPS spectra were processed using the Avantage software.

Raman spectra were recorded by Renishaw inVia QONTOR Raman microscope equipped with Leica microscope and a CCD detector using excitation wavelength of 532 nm, 20× objective and 1200 l/mm grating.

NMR spectra were measured using a Bruker 500 MHz NMR spectrometer with a cryoprobe broadband. For the analysis, 2 mL of electrolyte (post chronoamperometric measurements) was added to an NMR tube containing 90% electrolyte and 10% D_2O. Measurements were made using a water suppression technique developed by Bruker.

The HPLC was recorded on a Hewlett Packard Agilent 1100 series chromatograph equipped with an oven. 5 mL of the electrolyte after electrolysis at −0.3 V was injected into a ODS HYPERSIL column with a diameter of 250×4.6 mm. The column was heated to 60 °C and an eluent of 1 mM H_2SO_4 (in Millipore water) was used. A refractive index detector (RID) was used for product detection. Analytical standards consisting of 0.1 M acetic acid and formic acid were calibrated using the same method as mentioned above.

Results and Discussion

Characterization of Catalyst Material

The FTIR spectra (Figure 1) reveals the chemical identity of GO, TiO_2 as well as TiO_2/rGO and Cu-TiO_2/rGO composites. The GO spectrum shows typical vibrational groups associated with GO. These include the broad absorption peak between 3000 cm^{-1} and 3700 cm^{-1} (–OH stretching vibrations due to the presence of water molecules). Other peaks are also observed at 1052 cm^{-1} (C–O stretching of alkoxy groups), 1220 cm^{-1} (C–O–C stretching of epoxy groups), 1404 cm^{-1} (C–OH deformation), 1617 cm^{-1}.[34,35] The TiO_2 spectrum shows a broad peak centred at 3355 cm^{-1} and a low intensity peak at 1634 cm^{-1} which is attributed to surface adsorbed water and hydroxyl group (Ti–OH), respectively. The peaks below 800 cm^{-1} correspond to Ti–O modes (Ti–O and Ti-O–Ti stretching).[36]

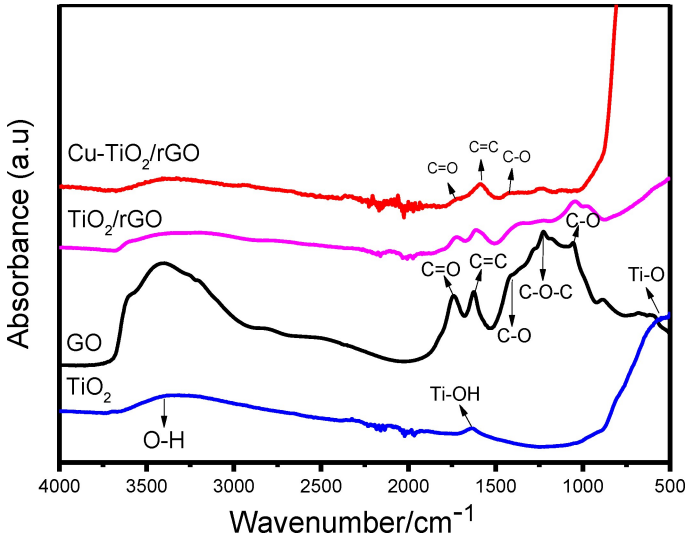

Figure 1. FTIR spectra of TiO_2, GO, TiO_2/rGO and Cu-TiO_2/rGO.

The spectrum of TiO_2/rGO and Cu-TiO_2/rGO shows that oxygen functionalities still exist on the surface of TiO_2/rGO and Cu-TiO_2/rGO although, a drastic reduction in the intensities is observed. This confirms the partial reduction of GO during synthesis of composites. The TiO_2/rGO spectrum shows a broad peak from 3000 cm^{-1} to 3672 cm^{-1} that represents O–H stretching. Other peaks at 1047 cm^{-1} (alkoxy C–O),[37] 1365 cm^{-1} (C–OH stretching of alkoxy and Ti–O modes), 1606 cm^{-1} (alkene C=C and Ti–OH)[38] and 1723 cm^{-1} (C=O stretching of carboxyl groups) from GO. In the Cu-TiO_2/rGO spectrum, the 1131 cm^{-1} (alkoxy), 1227 cm^{-1} (carboxyl), 1415 cm^{-1} (alkene), 1592 cm^{-1} (carbonyl) and 3353 cm^{-1} (hydroxyl groups) are observed with a shift in the vibrational frequencies indicating the formation of Cu-TiO_2/rGO.

The XRD patterns of TiO_2, TiO_2/rGO and Cu-TiO_2/rGO in the 2θ range 10° to 80° are represented in Figure 2. As observed, all synthesized catalysts showed the diffraction pattern of mixed TiO_2 comprising of both anatase at 2θ values of 25.2°, 37.6°, 48.0°, 53.7°, and 62.6°, corresponding to (101), (004), (200), (105) and (204) planes, respectively and rutile at 2θ values of 27.3°, 36.1°, 38.5°, 42,1° and 55.1° indexed to the (110), (101), (200), (111) and (211) plane respectively.[39] These values are in good accordance with the standard cards JCPDS card no. 21–1272 and 21–1276. The XRD pattern of GO at 2θ = 10.5° is not visible in TiO_2/rGO and Cu-TiO_2/rGO, this is a clear indication of the reduction of GO to rGO. The low intensity peak of graphene (002) at ~25° are overlapped with the TiO_2 (101) peak at ~26°. This phenomenon has been reported in earlier literature.[32] In the Cu-TiO_2/rGO pattern, no diffraction peaks of Cu at 2θ = 43°, 45° and 36° were observed; this is because of the low Cu loading on Cu-TiO_2/rGO. Hence, XPS was used to confirm the presence of Cu NPs in Cu-TiO_2/rGO (Figure 5).

Raman spectroscopy was used to provide additional information on the electronic structure of TiO_2 and GO (Figure 3) Changes in the Raman intensity gives details on defects and carbon-carbon interactions. TiO_2, TiO_2/rGO and Cu-TiO_2/rGO show the Raman active modes of the anatase structure of TiO_2

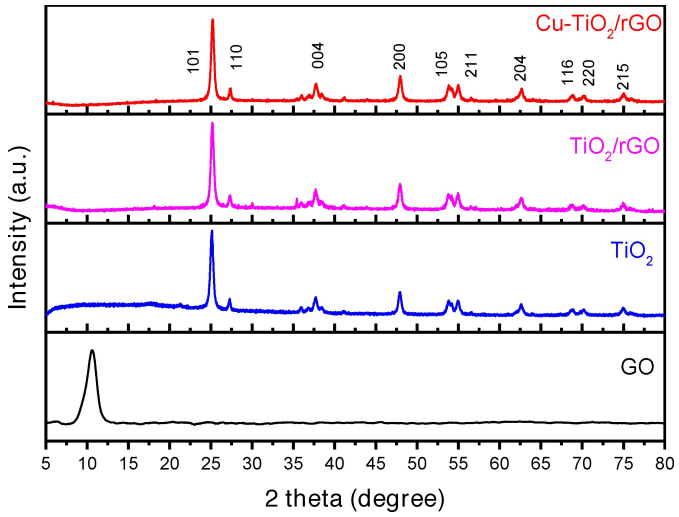

Figure 2. XRD patterns of GO, TiO_2, TiO_2/rGO and Cu-TiO_2/rGO.

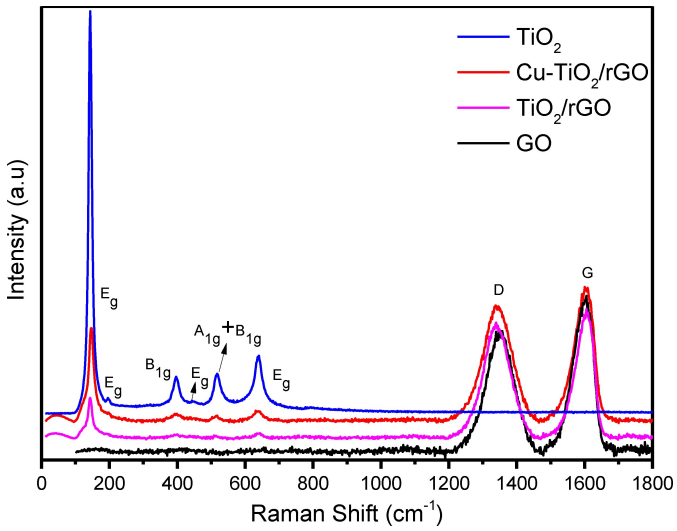

Figure 3. Raman spectra of GO, TiO_2, TiO_2/rGO and Cu-TiO_2/rGO.

at 144 cm^{-1} (E_g), 198 cm^{-1} (E_g), 396 cm^{-1} (B_{1g}), 516 cm^{-1} (A_{1g} + B_{1g}), and 640 cm^{-1} (E_g).[40–42] Furthermore, a weak Raman peak corresponding to the rutile structure of TiO_2 was observed at 445 cm^{-1} (E_g),[43,44] confirming the existence of TiO_2 in its anatase and rutile phase. This is in good agreement with the XRD analysis in Figure 2. The Raman spectrum of unmodified TiO_2 exhibits more intense peaks compared to the catalytic composites (TiO_2/rGO and Cu-TiO_2/rGO). A blue shift (of 1 cm^{-1}) in the E_g peak is observed for Cu-TiO_2/rGO, which is an indication of the strong interaction between Cu, TiO_2 and GO.

Two distinguished peaks located at 1351 cm^{-1} and 1603 cm^{-1} was observed across GO, TiO_2/rGO and Cu-TiO_2/rGO. These peaks correspond to the D-band and G-band of GO, respectively.[45,46] The D band corresponds to the out-of-plane sp^3 defects in the carbon skeleton while the G band corresponds to the in-plane vibrations of sp^2 graphitic carbons. The intensity ratio of the D to the G band (I_D/I_G) is a representation of the defects and grain size in graphene materials. A higher I_D/I_G value corresponds to an increase in the degree of disorderliness and an increase in the degree of aggregation.[47] An increase from 0.78 (GO) to 0.9 (TiO_2/rGO and Cu-TiO_2/rGO) in the calculated I_D/I_G ratio is observed in our measurements. This suggests a partial restoration and decrease in the size of available sp^2 domains as a result of fragmentation during the hydrothermal GO reduction. Hence, rGO layers are smaller in size and present in large quantities.[48]

The TEM images of TiO_2/rGO and Cu-TiO_2/rGO are presented in Figure 4. The images showed a two-dimensional wrinkled sheet, which is characteristic of rGO. It is evident in Figure 4a, b, c that TiO_2 and rGO have formed a composite where dark spherical/polygonal TiO_2 crystalline particles were homogenously distributed across the surface of bright thin fabric like rGO material. After the immobilization of pre-synthesized Cu NPs on TiO_2/rGO (Figure 4d, e, f), the dark spherical circles became slightly larger in number and deeply embedded in the polymer-like network (PVA) suggesting the presence of Cu NPs on TiO_2/rGO composite surface. In certain areas of the TEM survey, Cu NPs were completely submerged in TiO_2 particles,[49] making it difficult to distinguish their appearance. This was due to the well-known phenomenon that Cu NPs are often covered by a thin layer of Cu_2O due to atmospheric oxidation.[50] Thus, the image appearance was due to the mixed phases of Cu, Cu_2O and TiO_2. Also, the difference in atomic number between Cu (Z: 29) and Ti (Z: 22) is not large; hence the contrast between these two elements were not that obvious during the transmission of the electron beam. Thus, we can conclude from the TEM images that the 5–30 nm size of Cu/Cu_2O particles were embedded on TiO_2/rGO resulting in a hybrid composite.

XPS was used to determine the oxidation state of the metal components of Cu-TiO_2/rGO catalyst. Details of the deconvoluted and measured signals are represented in Figure 5. The full survey (Figure 5a) shows the elemental composition of Cu-TiO_2/rGO, from which the presence of Cu, Ti, O and C was confirmed. The core level spectra of Cu 2p (Figure 5b) was deconvoluted into two signals: Cu $2p_{3/2}$ and Cu $2p_{1/2}$. The Cu $2p_{3/2}$ signal was fitted into two peaks with binding energies at 932.5 eV and 934.7 eV corresponding to Cu^0 and Cu^+, respectively. In addition, the Cu $2p_{1/2}$ signal was fitted into two peaks with binding energies at 952.5 eV and 954.6 eV corresponding to Cu^0 and Cu^+, respectively. The absence of the shake-up satellite peak at 943.0 eV is a clear indication that Cu existed in the Cu^+ and Cu^0 oxidation states and not in Cu^{2+}.[51] Ti 2p core spectra (Figure 5c) was deconvoluted into two main peaks centred at 458.4 eV and 464.3 eV corresponding to Ti $2p_{3/2}$ and Ti $2p_{1/2}$, respectively. This is evidence of the existence of Ti in the +4-valence state. The additional peaks observed at 460.4 eV and

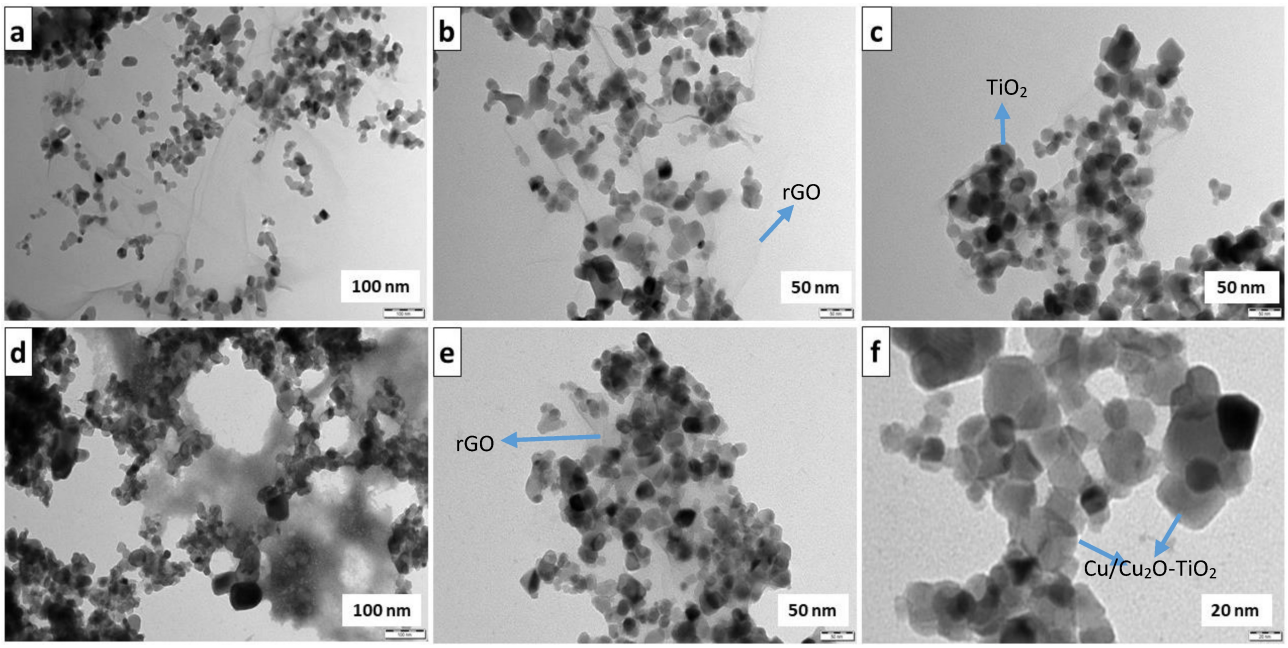

Figure 4. TEM images of TiO_2/rGO (a, b, c) and Cu-TiO_2/rGO (d, e, f).

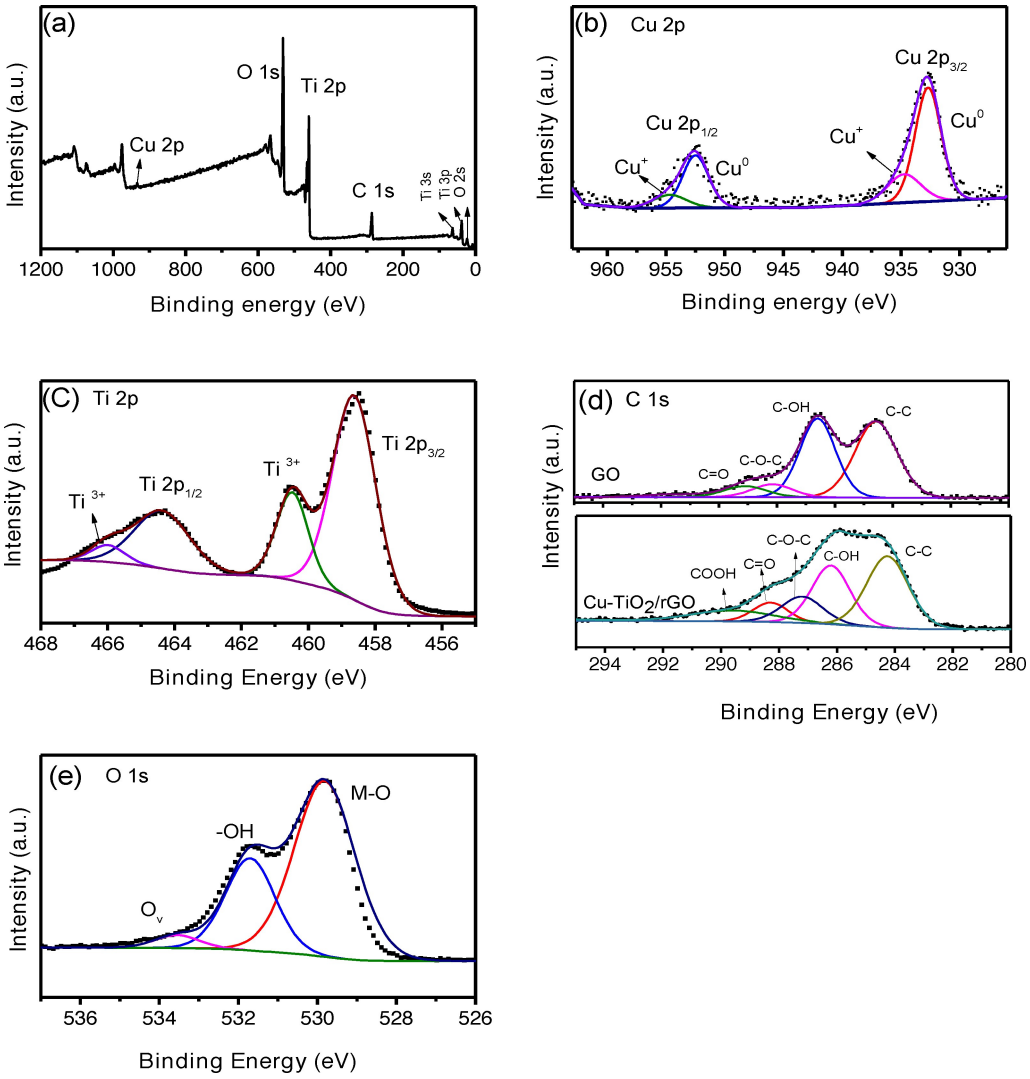

Figure 5. XPS full survey spectra of Cu-TiO_2/rGO (a) and deconvoluted Cu 2p (b), Ti 2p (c), C 1s (d) and O 1s (e).

466.4 eV corresponds to Ti in the +3-valence state. Therefore, the deconvoluted Ti 2p spectra highlights the existence of Ti in Ti^{3+} and Ti^{4+} oxidation state.[52,53] The peak at ≈460.0 eV also corresponds to literature values of a Ti–C bond, indicating a strong interaction between Ti and rGO.[54] The C 1s spectrum of GO and Cu-TiO_2/rGO is represented in Figure 5d. The C 1s spectrum of GO exhibited two intense and distinct peaks which is a characteristic of oxidation in GO. The deconvoluted C 1s signal of GO and Cu-TiO_2/rGO presented peaks corresponding to the sp^3 and partial sp^2 hybridization peak (C–C/C=C) at 284.2 eV. Other fitted peaks observed at 286.3, 287.1, 288.3 and 290 eV were assigned to oxygenated carbon (C–O), epoxide (C–O–C), and carbonyl (C=O, COOH) groups.[55] The O 1s core level spectra were deconvoluted into three peaks, as shown in Figure 5e. The peak, at 529.8 eV is attributed to the lattice oxygen in the metal (M–O).[56] The peak at 531.6 eV was assigned to –OH absorption[57] and the peak at 533.5 eV to the presence of oxygen vacancies (O_V).[58]

Electrocatalytic Activity of Catalyst Materials Towards CO_2 Reduction

The $ERCO_2$ was initially studied by linear sweep voltammetry (LSV) using TiO_2, TiO_2/rGO, and Cu-TiO_2/rGO nanocomposites in N_2 and CO_2 saturated 0.5 M $KHCO_3$ using the rotating disc electrode (RDE, the Pt ring was turned off) at a scan rate of 100 mVs^{-1}, rotational speed of 1600 rpm and a potential range from 0.4 to −0.6 V *vs* RHE. This potential range was the most suitable for the determination of our desired product (acetic acid). As observed in Figure 6(a–c), the cathodic current densities of all catalyst materials increased in CO_2 saturated solution (solid line) as compared to N_2 saturated solution (dotted line). The increase in current density observed in N_2 saturated 0.5 M $KHCO_3$ solution can be attributed to hydrogen evolution reaction (HER). Thus, the higher current density observed in CO_2 saturated solution is a clear indication that $ERCO_2$ is more favourable than the HER on all catalyst materials. An onset reduction potential of −0.1 V, −0.3 V, and 0.1 V vs RHE was observed for TiO_2, TiO_2/rGO, and Cu-TiO_2/rGO,

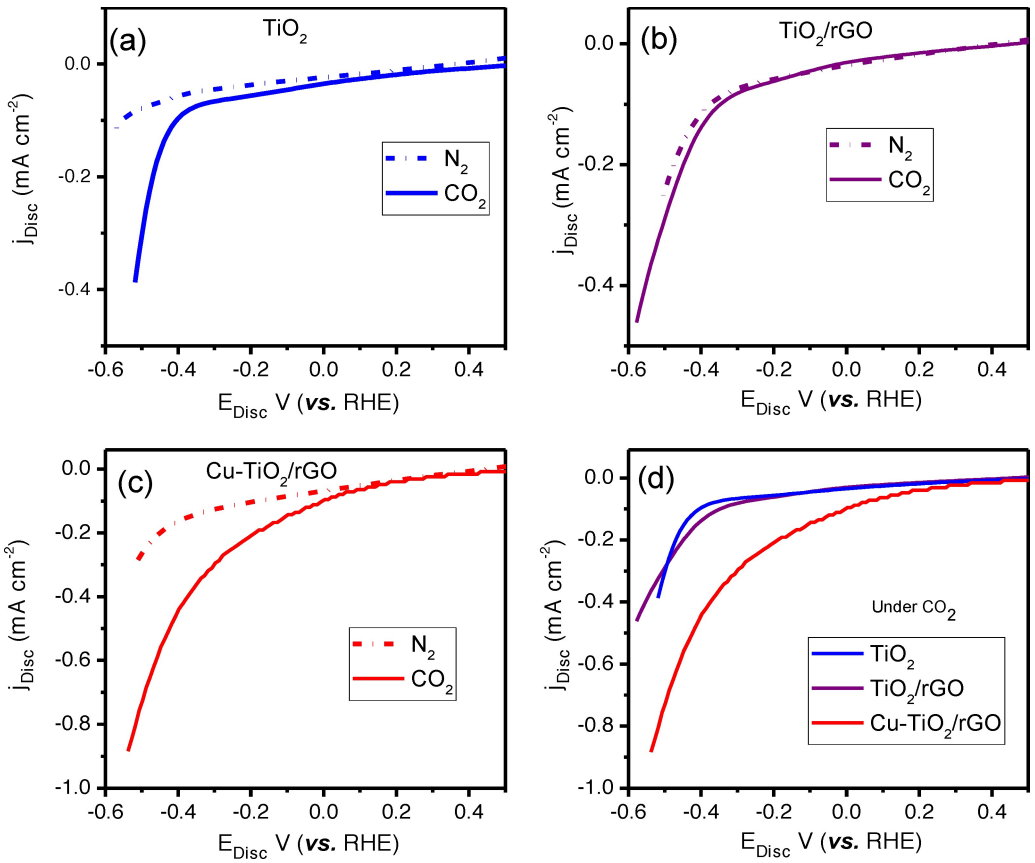

Figure 6. RDE LSV curves of (a) TiO_2 (b) TiO_2/rGO (c) Cu-TiO_2/rGO in N_2 and CO_2 saturated 0.5 M $KHCO_3$ (d) comparative plot of all three catalysts under CO_2 saturation. At a rotation speed of 1600 rpm, a scan rate of 100 mVs^{-1} (ring: off). The dotted lines denote N_2 saturation while the solid line denotes CO_2 saturation.

respectively. It is evident from Figure 6(d), that Cu-TiO_2/rGO exhibits a higher catalytic performance with an earlier onset (more positive) reduction potential and higher current density as compared to TiO_2 and TiO_2/rGO. This is a clear indication that embedding Cu NPs on TiO_2/rGO improves its electrocatalytic activity in $ERCO_2$. This is due to a combination of the available adsorption sites provided by the surface exposed atom of Cu nanoparticles, Cu/Cu_2O interface, and high electrical conductivity provided by the synergy between Cu, TiO_2 and defective GO sheets. The onset potential (0.1 V *vs.* RHE) observed for the $ERCO_2$ over Cu-TiO_2/rGO, corresponds with the already reported equilibrium potential for $ERCO_2$ to acetic acid as seen in (Eq. (3)) below.[59]

$$2CO_2 + 8H^+ + 8e^- \rightarrow CH_3COOH + 2H_2O \ (0.11\ V\ vs.\ RHE) \quad (3)$$

To conduct a more comprehensive evaluation of $ERCO_2$ product formation on the Cu-TiO_2/rGO nanocomposite, electrochemical investigations were performed using the RRDE.

Electrochemical Calibration on the Pt Ring

Prior to the product calibration on the Pt ring, electrochemical studies was conducted using the rotating ring electrode (RRE, the disc was turned off), to identify the potentials corresponding to Pt oxidation and reduction in CO_2 saturated 0.5 M $KHCO_3$ at a scan rate of 100 mVs^{-1} and a rotation of 1600 rpm (Figure S1). As observed in the anodic scan of the corresponding RRE CV, an onset potential of 1.36 V corresponds to Pt oxide formation. While on the cathodic scan, the reduction of the oxide begins at 0.2 V with a peak maximum at 0.17 V. The calibration of product species (0.1 M AA/CO_2 and 0.1 M FA/CO_2) is represented in Figure 7. As observed, 0.1 M AA/CO_2 (Figure 7(a)) is characterized by a broad peak (from 0.83 to 1.35) V *vs.* RHE with a lower current density compared to the blank CO_2 saturated electrolyte. Literature report by Zuo *et al.* has established a pH dependent adsorption of acetate on Pt electrode.[60] Similar to Figure 7(a), Zuo *et al.* observed the disappearance/suppression of the characteristic Pt oxide peak due to the adsorption of acetate at pH 7.6 and lower. Thus, although a small current density is observed with the 0.1 M AA/CO_2 solution, a peak centred at 1.22 V *vs.* RHE is observed. In Figure 7(b), the Pt ring response to 0.1 M FA/CO_2 mixture is characterized with three anodic peaks (two on the forward scan and one on the reverse scan). The first wide anodic peak centred at 0.8 V *vs.* RHE (forward scan) corresponds to the direct oxidation of FA. The second anodic peak at 1.33 V *vs.* RHE (forward scan) corresponds to the oxidative removal of CO. An

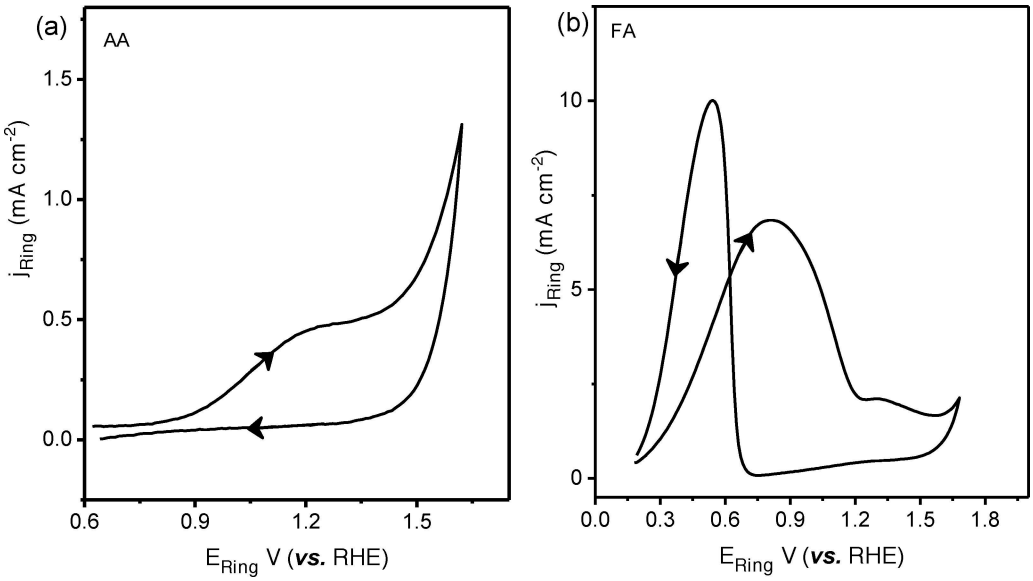

Figure 7. RRE CV calibration scan on the Pt ring of (a) Acetic acid (b) Formic acid in CO_2 saturated 0.5 M $KHCO_3$ at a rotation speed of 1600 rpm and a scan rate of 100 mVs^{-1} (disc: off). The arrows indicate the scan direction.

additional anodic peak (reverse scan) is observed at 0.55 V *vs.* RHE.[61,62]

$ERCO_2$ In Situ Detection on Pt Ring

The second set of experiment involved an *in situ* detection of products formed during $ERCO_2$ in 0.5 M $KHCO_3$ on Cu-TiO_2/rGO catalyst (Figure 8). The ring was scanned from 0.6 to 1.7 V *vs.* RHE at a scan rate of 100 mVs^{-1} and a rotation speed of 1600 rpm while keeping the disc at relevant reductive potentials where $ERCO_2$ is expected to generate products. As concluded from Figure 6(c), an onset positive potential of 0.11 V was observed for $ERCO_2$ on Cu-TiO_2/rGO. Thus, constant potentials close to 0.11 V was applied to the disc (E_{disc}) at 0.1 interval (−0.1 V, −0.2 V, −0.3 V and −0.4 V) in CO_2 saturated 0.5 M $KHCO_3$. Figure 8 compares (i) the CV scans obtained on the Pt ring while the disc (containing Cu-TiO_2/rGO catalyst) was subjected to constant potentials and (ii) the Pt ring calibration scan of 0.1 M AA/CO_2. An oxidation peak broadening from 0.83 V to 1.35 V with a slight shift in peak maximum at 1.2 V *vs.* RHE is evident across all E_{disc} potentials. This broad peak is the only peak observed on the Pt ring, and it is comparable to the CV curve obtained for 0.1 M AA/CO_2, indicating the desired eight electron pathway for the formation of acetic acid (Eq. (3)). However, no peak corresponding to 0.1 M FA/CO_2 (Figure 7) was observed on the Pt ring in Figure 8, thus confirming that the $ERCO_2$ using the synthesized Cu-TiO_2/rGO catalyst yields mainly AA. However, a positive shift in the oxidation peak maximum is evident at potentials less than −0.3 V (E_{disc} < −0.3 V), this could be attributed to the formation of AA and other gaseous intermediates. AA formation is predominant at E_{disc} −0.3 V, with a current density of 0.45 mAcm^{-2}. It is noteworthy that at potentials above −0.3 V (E_{disc} > −0.3 V), a

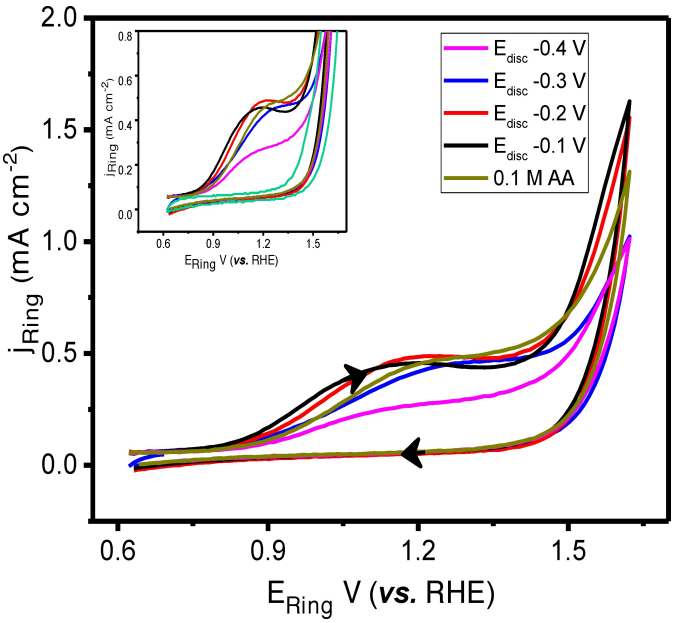

Figure 8. RRDE CV scan at the Pt ring using the Cu-TiO_2/rGO modified GC disc electrode in CO_2 saturated 0.5 M $KHCO_3$ at a scan rate of 100 mVs^{-1} and rotation speed of 1600 rpm. The constant potentials applied to the disc are indicated in the graph. RRDE CV of the bare Pt ring is indicated by the green line in the inset. The arrows indicate the scan direction.

decline in AA formation was observed. Particularly, lower current response was observed at E_{disc}−0.4 V. The formation of AA at less negative potentials (−0.1 V to −0.4 V) *vs.* RHE is in good agreement with literature where $ERCO_2$ at Cu-based electrodes have yielded acetate/acetic acid.[16,63–65] Table 1 presents a comparison of our experimental data on $ERCO_2$ to acetic acid with some of those in existing literature.

Thus, our RRDE experiments confirm a selective hydrogenation of CO_2 into CH_3COOH through a C–C bond formation,

Table 1. Comparison of various Cu-based catalyst for the $ERCO_2$ towards the formation of acetate/acetic acid.

catalyst	Electrolyte	Applied Potential (V)	Reference
$CuGa_2$	0.5 M $KHCO_3$	−0.1 (*vs.* RHE)	[63]
Cu_2O-Cu^0/CP	0.3 M $KHCO_3$	−0.4 (*vs.* RHE)	[64]
PcCu-TFPN	0.1 M $KHCO_3$	−0.8 (*vs.* RHE)	[65]
Cu-Cu_2O/Cu	0.1 M KCl	−0.4 (*vs.* RHE)	[16]
Cu-TiO_2/rGO	0.5 M $KHCO_3$	−0.3 (*vs.* RHE)	This work
Cu-TiO_2/rGO	0.5 M $KHCO_3$	−0.2 (*vs.* RHE)	This work
Cu-TiO_2/rGO	0.5 M $KHCO_3$	−0.1 (*vs.* RHE)	This work

on our well-designed electrocatalyst material, Cu-TiO_2/rGO. It is noteworthy that product formation using this method can then be tuned for selectivity by adjusting the potential applied on the disc. Although the major focus of this study was on product detection and not quantification, it is interesting to note that a few literature reports have employed the RRDE for product quantification by applying the formula indicated in (Eq. (4)) below.[28]

$$FE_{RRDE} = \frac{i_R}{|i_D|N}^{*} 100 \quad (4)$$

We explored the RRDE as a tool to calculate faradaic efficiency using (Eq. (4)). Linear voltammetry was carried out on the disc while keeping the ring at the catalytically relevant oxidative potential (1.2 V *vs.* RHE) as established in Figure 7(a) and Figure 8. The corresponding disc (i_D) and ring (i_R) current at selected potentials were collected, along with the N value (0.3). These values were subsequently employed in the calculation of the total FE for $ERCO_2$ (Figure 9). As observed in Figure 9, the highest FE was recorded at −0.1 V (22%), and the total FE decreases as the disc potential becomes more negative. The low total FE observed could be a result of the diffusion limitation of the RRDE to completely sweep all products to the ring for detection, which results in the low FE of desired products. The calculated FE was ascribed mainly to the formation of acetic acid with some contribution of other gaseous intermediates.

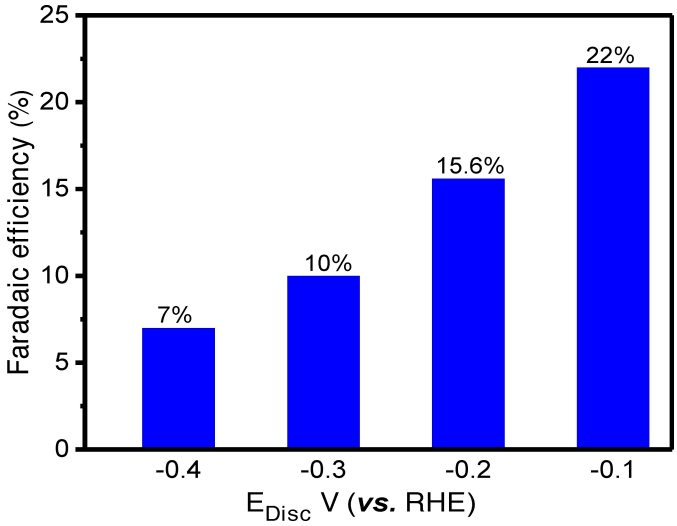

Figure 9. Total faradaic efficiency of $ERCO_2$ on Cu-TiO_2/rGO using RRDE.

To further validate the identity of the product generated from the $ERCO_2$, chronoamperometric electrolysis of the catalytically relevant potential (−0.3 V) was performed on the Cu-TiO_2/rGO modified GC disc electrode and the aliquot was analysed using NMR and HPLC. The rotating disc electrode (RDE) technique was used at a rotation speed of 1600 rpm and potential was maintained at E_{disc}−0.3 V *vs.* RHE for 60 min. The chromatogram (HPLC) of the aliquot was qualitatively interpreted in comparison with the HPLC calibration of 0.1 M FA and 0.1 M AA (Fig S2). An increase in the expected peak corresponding to AA was observed, thus validating the presence of AA in the aliquot. The NMR was also employed for product detection and identification (Fig S3). 1H NMR spectra also exhibits chemical shift corresponding to AA. Therefore, $ERCO_2$ to AA was confirmed using the NMR and HPLC. Although these traditional methods were not employed for quantification in this research, they still served as a valuable support to confirm the identity of the product generated. The comparability of the product detection of the RRDE to the other traditional non-electrochemical techniques (NMR and HPLC) makes it a cost-effective tool for electrochemical applications. This therefore demonstrates the superior sensitivity and detection capability of the RRDE.

Conclusions

In this study, electrocatalyst consisting of metal nanoparticles was synthesized and their catalytical activity towards $ERCO_2$ was evaluated. Cu-TiO_2/rGO showed superior performance in comparison to the support materials, with a lower onset reduction potential of 0.1 V *vs.* RHE. The improved performance of Cu-TiO_2/rGO as compared to TiO_2 and TiO_2/rGO was attributed to the combination of a) metallic active sites of Cu b) surface exposed atoms on thin layer of Cu_2O c) interfaces between Cu and Cu_2O d) synergistic effect between Cu and TiO_2/ rGO which eventually enhanced the catalytic activity in $ERCO_2$. This study further presented the RRDE as a unique electroanalytical tool for the investigation of product generated during $ERCO_2$ on the Cu-TiO_2/rGO catalyst. The Cu-TiO_2/rGO catalyst demonstrated selective reduction of CO_2 to mainly AA at −0.1 V, −0.2 V, and −0.3 V *vs.* RHE. The highest total faradaic efficiency of $ERCO_2$ was empirically calculated to be 22% at −0.1 V *vs.* RHE. The RRDE result was compared with conventional non-electrochemical techniques (NMR and HPLC), and the formation of AA was validated. Thus, RRDE demonstrated improved detection capability, indicating its suitability as a rapid, sensitive, and unique *in situ* tool for the identification of products generated during $ERCO_2$ and other electrochemical applications. The experimental conclusions in this study, displays the effectiveness of the Cu-TiO_2/rGO electrocatalyst and the RRDE technique,

in broadening the scope for the selective hydrogenation of CO_2 while enabling value-added recycling.

Acknowledgements

A.O.K acknowledges: (i) University of Turku Graduate School (UTUGS), (ii) Doctoral Programme in Exact Sciences (EXACTUS), and (iii) Magnus Ehrnrooth Foundation for financial support. L.K thanks Turku Collegium for Science & Medicine (TCSM) and Finnish Cultural Foundation (SKA) for funding. We thank the Electron Microscopy Laboratory, Institute of Biomedicine, University of Turku and Biocenter Finland for the TEM analysis. Further, we thank the MATSURF consortium for XPS analysis. Mauri Nauma is acknowledged for technical help with cell designs and modifications. Lange Saleh and Mark Afari are appreciated for help during HPLC measurement.

Conflict of Interests

The authors declare no conflict of interest.

Data Availability Statement

The data that support the findings of this study are available from the corresponding author upon reasonable request.

Keywords: Heterogenous Cu-TiO_2/rGO · composite electrode · RRDE · CO_2 reduction · electrocatalysis · carboxylic acid products · CO_2 recycling and value addition

[1] F. Zhang, A. C. Co, *J. Electrochem. Soc.* **2020**, *167*, 046517.
[2] E. Ruiz-López, J. Gandara-Loe, F. Baena-Moreno, T. R. Reina, J. A. Odriozola, *Renewable Sustainable Energy Rev.* **2022**, *161*, 112329.
[3] R. Nazir, A. Kumar, M. A. Saleh Saad, A. Ashok, *Colloids Surf A Physicochem Eng Asp* **2020**, *598*, 124835.
[4] A. R. Haines, J. C. Hemminger, *ACS Catal.* **2021**, *11*, 6960–6970.
[5] F. Yang, C. Jiang, M. Ma, F. Shu, X. Mao, W. Yu, J. Wang, Z. Zeng, S. Deng, *Chem. Eng. J.* **2020**, *400*, 125879.
[6] E. Hajialilou, H. Asgharzadeh, S. Khameneh Asl, *Appl. Surf. Sci.* **2021**, *544*, 148832.
[7] J. Yuan, J. J. Zhang, M. P. Yang, W. J. Meng, H. Wang, J. X. Lu, *Catalysts* **2018**, **2018**, *8*, 171.
[8] N. Rashid, M. A. Bhat, U. K. Goutam, P. P. Ingole, *RSC Adv* **2020**, *10*, 17572–17581.
[9] N. Altaf, S. Liang, R. Iqbal, M. Hayat, T. R. Reina, Q. Wang, *J. CO2 Util.* **2020**, *40*, 101205.
[10] B. Srinivas, B. Shubhamangala, K. Lalitha, P. Anil Kumar Reddy, V. Durga Kumari, M. Subrahmanyam, B. R. De, *Photochem. Photobiol.* **2011**, *87*, 995–1001.
[11] J. Albo, A. Sáez, J. Solla-Gullón, V. Montiel, A. Irabien, *Appl. Catal. B* **2015**, *176–177*, 709–717.
[12] A. Adamu, M. Isaacs, K. Boodhoo, F. R. Abegão, *J. CO2 Util.* **2023**, *70*, 102428.
[13] K. P. Kuhl, E. R. Cave, D. N. Abram, T. F. Jaramillo, *Energy Environ. Sci.* **2012**, *5*, 7050–7059.
[14] T. Ma, Q. Fan, X. Li, J. Qiu, T. Wu, Z. Sun, *J. CO2 Util.* **2019**, *30*, 168–182.
[15] C. Genovese, C. Ampelli, S. Perathoner, G. Centi, *Green Chem.* **2017**, *19*, 2406–2415.
[16] Q. Zhu, X. Sun, D. Yang, J. Ma, X. Kang, L. Zheng, J. Zhang, Z. Wu, B. Han, *Nature Communications* **2019**, *10*, 1–11.
[17] W. Ahmad, P. Koley, S. Dwivedi, R. Lakshman, Y. K. Shin, A. C. T. van Duin, A. Shrotri, A. Tanksale, *Nat. Commun.* **2023**, *14*, 2821.
[18] L. Wang, K. Gupta, J. B. M. Goodall, J. A. Darr, K. B. Holt, *Faraday Discuss.* **2017**, *197*, 517–532.
[19] M. Papasizza, A. Cuesta, *ACS Catal.* **2018**, *8*, 6345–6352.
[20] J. Heyes, M. Dunwell, B. Xu, *J. Phys. Chem. C* **2016**, *120*, 17334–17341.
[21] G. Marcandalli, M. C. O. Monteiro, A. Goyal, M. T. M. Koper, *Acc. Chem. Res.* **2022**, *55*, 1900–1911.
[22] G. Marcandalli, A. Goyal, M. T. M. Koper, *ACS Catal.* **2021**, *11*, 4936–4945.
[23] D. M. Harraz, S. Weng, Y. Surendranath, *ACS Catal.* **2023**, *13*, 1462–1469.
[24] A. Kerschbaumer, D. Wielend, E. Leeb, C. Schimanofsky, N. Kleinbruckner, H. Neugebauer, M. Irimia-Vladu, N. S. Sariciftci, *Catal. Sci. Technol.* **2023**, *13*, 834–843.
[25] J. Jia, H. Yang, G. Wang, P. Huang, P. Cai, Z. Wen, *ChemElectroChem* **2018**, *5*, 471–477.
[26] R. E. Vos, M. T. M. Koper, *ChemElectroChem* **2022**, *9*, e202200239.
[27] X. Liu, M. T. M. Koper, *J. Am. Chem. Soc.* **2024**, *146*, 5242–5251.
[28] J. F. Z. Cardona, J. Sacanell, M. A. Barral, V. Vildosola, F. A. Viva, *J. CO2 Util.* **2022**, *59*, 101973.
[29] X. Zhu, K. Gupta, M. Bersani, J. A. Darr, P. R. Shearing, D. J. L. Brett, *Electrochim. Acta* **2018**, *283*, 1037–1044.
[30] M. Hirata, T. Gotou, S. Horiuchi, M. Fujiwara, M. Ohba, *Carbon N Y* **2004**, *42*, 2929–2937.
[31] P. Damlin, M. Suominen, M. Heinonen, C. Kvarnström, *Carbon N Y* **2015**, *93*, 533–543.
[32] S. D. Perera, R. G. Mariano, K. Vu, N. Nour, O. Seitz, Y. Chabal, K. J. Balkus, *ACS Catal.* **2012**, *2*, 949–956.
[33] A. O. Koyejo, L. Kesavan, P. Damlin, M. Salomäki, J. G. Yao, M. Hakkarainen, C. Kvarnström, *ChemElectroChem* **2020**, *7*, 4889–4899.
[34] V. C. Nguyen, S. Kheireddine, A. Dandach, M. Eternot, T. T. H. Vu, N. Essayem, *Catalysts* **2020**, *10*, 1393.
[35] D. Yang, D. Yang, *Titanium Dioxide - Material for a Sustainable Environment* **2018**, DOI 10.5772/INTECHOPEN.70290.
[36] G. Wang, L. Xu, J. Zhang, T. Yin, D. Han, *Int. J. Photoenergy* **2012**, *2012*, 265760.
[37] N. Lertthanaphol, N. Pienutsa, K. Chusri, T. Sornsuchat, P. Chanthara, P. Seeharaj, P. Kim-Lohsoontorn, S. Srinives, *ACS Omega* **2021**, *6*, 35769–35779.
[38] S. A. Khan, Z. Arshad, S. Shahid, I. Arshad, K. Rizwan, M. Sher, U. Fatima, *Compos. B. Eng.* **2019**, *175*, 107120.
[39] A. O. Koyejo, L. Kesavan, P. Damlin, M. Salomäki, C. Kvarnström, *ChemElectroChem* **2022**, *9*, e202200442.
[40] J. Bansal, R. Tabassum, S. K. Swami, S. Bishnoi, P. Vashishtha, G. Gupta, S. N. Sharma, A. K. Hafiz, *Appl. Phys. A Mater. Sci. Process.* **2020**, *126*, 1–10.
[41] G. T. S. How, A. Pandikumar, H. N. Ming, L. H. Ngee, *Sci. Rep.* **2014**, *4*, 1–8.
[42] F. D. Hardcastle, *J Ark Acad Sci* **2011**, *65*, 43–48.
[43] A. Pandikumar, R. Ramaraj, *Journal of Renewable and Sustainable Energy* **2013**, *5*, 043101.
[44] O. Zakir, A. Ait Karra, R. Idouhli, M. Elyaagoubi, M. Khadiri, B. Dikici, A. Aityoub, A. Abouelfida, A. Outzourhit, *J. Solid State Electrochem.* **2022**, *26*, 2247–2260.
[45] H. Zhang, X. Wang, N. Li, J. Xia, Q. Meng, J. Ding, J. Lu, *RSC Adv.* **2018**, *8*, 34241–34251.
[46] Y. Gong, D. Li, Q. Fu, C. Pan, *Prog. Nat. Sci.* **2015**, *25*, 379–385.
[47] L. Wu, M. Li, M. Li, Q. Sun, C. Zhang, *Polymers (Basel).* **2020**, *12*, 1426.
[48] K. Dong, J. He, J. Liu, F. Li, L. Yu, Y. Zhang, X. Zhou, H. Ma, *J. Mater. Sci.* **2017**, *52*, 6754–6766.
[49] K. Sekar, C. Chuaicham, B. Vellaichamy, W. Li, W. Zhuang, X. Lu, B. Ohtani, K. Sasaki, *Appl. Catal. B* **2021**, *294*, 120221.
[50] M. B. Gawande, A. Goswami, F. X. Felpin, T. Asefa, X. Huang, R. Silva, X. Zou, R. Zboril, R. S. Varma, *Chem. Rev.* **2016**, *116*, 3722–3811.
[51] J. Li, Z. Mei, L. Liu, H. Liang, A. Azarov, A. Kuznetsov, Y. Liu, A. Ji, Q. Meng, X. Du, *Sci. Rep.* **2014**, *4*, 7240.
[52] W.-C. Peng, Y.-C. Chen, J.-L. He, S.-L. Ou, R.-H. Horng, D.-S. Wuu, *Sci. Rep.* **2018**, *8*, 9255.
[53] D. Vasu, A. Karthi Keyan, S. Sakthinathan, T. W. Chiu, *Sci. Rep.* **2022**, *12*, 886.
[54] S. G. Babu, R. Vinoth, D. Praveen Kumar, M. V. Shankar, H. L. Chou, K. Vinodgopal, B. Neppolian, *Nanoscale* **2015**, *7*, 7849–7857.
[55] M. Zong, Y. Huang, H. Wu, Y. Zhao, P. Liu, L. Wang, *Mater. Lett.* **2013**, *109*, 112–115.
[56] W. Xie, R. Li, Q. Xu, *Sci. Rep.* **2018**, *8*, 8752.

[57] T. Zhang, T. Yang, S. Huang, Y. Pu, S. Wei, W. Gao, *J. Mater. Sci.* **2022**, *57*, 2455–2466.
[58] A. Devadoss, P. Sudhagar, C. Ravidhas, R. Hishinuma, C. Terashima, K. Nakata, T. Kondo, I. Shitanda, M. Yuasa, A. Fujishima, *Phys. Chem. Chem. Phys.* **2014**, *16*, 21237–21242.
[59] S. Hui, N. Shaigan, V. Neburchilov, L. Zhang, K. Malek, M. Eikerling, P. De Luna, *Nanomaterials* **2020**, *10*, 1–53.
[60] X. Q. Zuo, W. Chen, A. Yu, M. Le Xu, J. Cai, Y. X. Chen, *Electrochem. Commun.* **2018**, *89*, 6–9.
[61] I. M. Al-Akraa, A. E. Salama, Y. M. Asal, A. M. Mohammad, *Arab. J. Chem.* **2021**, *14*, 103383.
[62] Q. Yi, A. Chen, W. Huang, J. Zhang, X. Liu, G. Xu, Z. Zhou, *Electrochem. Commun.* **2007**, *9*, 1513–1518.
[63] D. Bagchi, J. Raj, A. K. Singh, A. Cherevotan, S. Roy, K. S. Manoj, C. P. Vinod, S. C. Peter, D. Bagchi, J. Raj, A. Cherevotan, S. Roy, K. S. Manoj, S. C. Peter, A. K. Singh, *Adv. Mater.* **2022**, *34*, 2109426.
[64] M. Serafini, F. Mariani, A. Fasolini, E. Scavetta, F. Basile, D. Tonelli, *Cite This: ACS Appl. Mater. Interfaces* **2021**, *13*, 57461.
[65] X.-F. Qiu, J.-R. Huang, C. Yu, Z.-H. Zhao, H.-L. Zhu, Z. Ke, P.-Q. Liao, X.-M. Chen, *Angew. Chem.* **2022**, *134*, e202206470.

Manuscript received: March 11, 2024
Revised manuscript received: April 29, 2024